Special Issue: Earthquake geology

Rock-falls and liquefaction related phenomena triggered by the June 8, 2008, M_w=6.4 earthquake in NW Peloponnesus, Greece

Spyros Pavlides[1], George Papathanassiou[1,*], Sotiris Valkaniotis[1], Alexis Chatzipetros[1], Sotiris Sboras[1,2], Riccardo Caputo[2]

[1] *Aristotle University of Thessaloniki, Department of Geology, Thessaloniki, Greece*

[2] *Università degli Studi di Ferrara, Dipartimento di Fisica e Scienze della Terra, Ferrara, Italy*

Article history
Received May 31, 2012; accepted November 4, 2013.
Subject classification:
Earthquake, Rock-falls, Liquefaction, Greece, Peloponnesus.

ABSTRACT

A strong earthquake (M_w=6.4) occurred in NW Peloponnesus, Greece, on June 8, 2008. The focal mechanism shows a transcurrent kinematics, and based on aftershocks distribution the causative fault is a dextral strike-slip NNE-SSW trending structure. The shock generated severe secondary environmental effects like rock-falls and liquefaction phenomena inducing structural damages and ground failures mainly along the fault strike. Evidence of liquefaction was observed in the area of Kato Achaia and Roupakia villages, while rock-falls were triggered mainly close to the epicentre at the foothills of the Skolis Mountain. Based on a quantitative methodological approach, the ground deformation and failures generated by the event have been investigated. In particular, based on an immediate post-event survey, we mapped in detail the distribution of the earthquake-induced ground failures, defining the areas prone to liquefaction and their associated potential. Moreover, a rock-fall hazard zonation in the area of Skolis Mountain has been developed based on the shadow angle approach, confirming the validity of the safety run-out distance models.

1. Introduction

On Sunday June 8, 2008 (12:25 GMT; 15:25 local time), a strong earthquake (M_w=6.4) affected the NW Peloponnesus, Greece, inducing several earthquake environmental effects and structural damages in the broader epicentral area (Figure 1). According to the Institute of Geodynamics of the National Observatory of Athens (NOA), the focus was at 37.98°N, 21.51°E and 25 km-deep (/www.gein.noa.gr/services/Noa_cat/CAT2003.txt). However, the Seismological station of the Aristotle University of Thessaloniki provided slightly different coordinates (37.963°N, 21.525°E and 16 km hypocentral depth; /geophysics.geo.auth.gr/ss/). Based on a refinement of the velocity model, the hypocenter was subsequently relocated at 18 km [Kostantinou et al. 2009]. All the focal mechanisms show an almost purely transcurrent kinematics [e.g. Gallovic et al. 2009, Ganas et al. 2009, Papadopoulos et al. 2010, Kostantinou et al. 2011], while according to aftershock distribution and DInSAR analyses, the causative fault was the NNE-SSW trending dextral strike-slip plane [Chouliaras 2009, Ganas et al. 2009, Kostantinou et al. 2009, Feng et al. 2010, Papadopoulos et al. 2010]. Likely due to the focal depth, the seismogenic fault remained blind and no coseismic surface ruptures formed.

Notwithstanding, the secondary environmental effects triggered by the event were spread over a wide area of northwestern Peloponnesus extending from Kato Achaia, to the north, to Amaliada, to the south. The most severe damages were reported along the surface projection of the fault (i.e. in a NNE-SSW elongated area). In particular, landslides were observed close to the epicentre, at Valmi village, while rock-falls were observed at the villages of Santomeri and Portes affecting roads and houses, respectively. Ground ruptures with mainly extensional kinematics (opening and up to 20 cm of throw) and locally with a slight strike-slip component (maximum 15 cm horizontal displacement) were observed close to the village of Nisi, causing also minor damages to a local bridge.

Few days after the event, a detailed field survey took place by our team in order to observe and measure all possible ground effects induced by the earthquake. Indeed, the main goal was to provide quantitative information about the occurred surficial phenomena. In particular, we analyzed the volume of several rock-falls and the grain size characteristics of the ejected material due to soil liquefaction. As a major outcome we

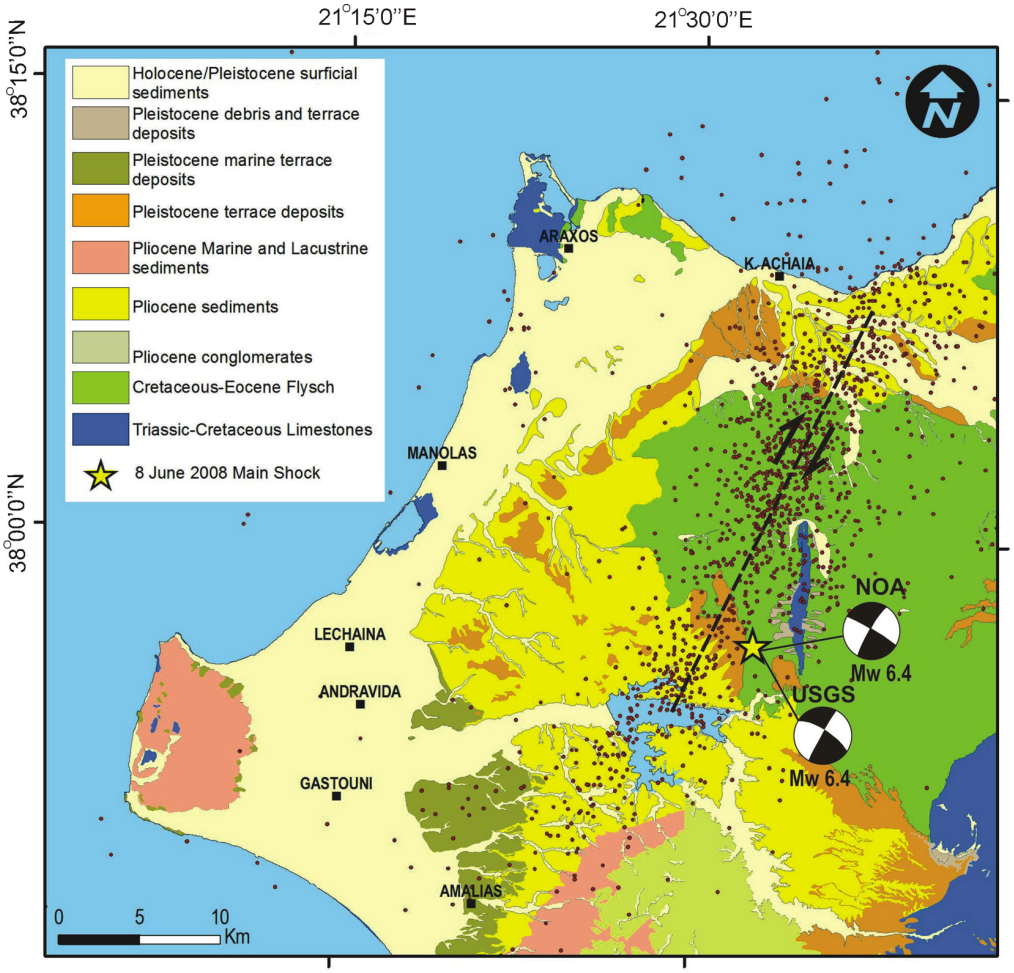

Figure 1. Simplified geological map of the study area showing the location of the seismogenic fault as it was defined by the focal mechanisms and the alignment of aftershocks from June 8 to 16, 2008.

produce maps showing the distribution of earthquake-induced ground failures and the distribution of the earthquake intensity evaluated on the basis of the ESI-2007 scale [Michetti et al. 2007]. For the foothills area of Skolis Mountain, we also prepared rock-fall hazard maps based on run-out distances approaches and the results are compared with the effects induced by the 2008 earthquake.

2. Geological and seismotectonic setting

From a geodynamic point of view, the epicentral area belongs to the External Hellenides and mainly affected the Ionian and Gavrovo zones [Fleury et al. 1981, Kamberis et al. 2000]. Within the epicentral area, the contact between the two major tectonic units outcrops along the western side of the Skolis Mountain (Figure 1), where westwards thrusting juxtaposes the Tithonian-to-Eocene neritic carbonates belonging to the Gavrovo Zone, to the east, onto the Ionian flysch, to the west [Kamberis et al. 2000].

The overall present-day setting of the area is mainly the result of the Oligocene to Pliocene thin- and thick-skin tectonics which occurred at shallow and deep crustal levels, respectively [Kokkalas et al. 2013]. Indeed, during collision, the Gavrovo Zone largely overthrusted the Ionian Zone by means of a crustal-scale detachment thus generating a doubling of the sedimentary successions. During this phase, the thick sequence of Triassic evaporites played a crucial role. In the late collisional stages an intense internal deformation occurred activating several out-of-sequence thrusts and back-thrusts, diapiric phenomena and the formation of sedimentary basins covering large sectors of NW Peloponnesus [e.g. Kamberis et al. 2000, Mavromatidis 2009]. These formations mainly of Pliocene-Pleistocene age, consist of sands, shales, clays, marls, limestones and conglomerates, deposited in shallow marine-littoral and lacustrine environment and may reach a local thickness greater than 1 km [Tsoflias 1970, Hageman 1976, Fleury et al. 1981].

As concerns the present-day stress regime, the broader region represents a transitional zone between the Corinth Gulf, undergoing N-S crustal stretching, and the collision-subduction regime persisting along the north-western sector of the Hellenic Arc [e.g. Benetatos et al. 2004]. Although these areas are character-

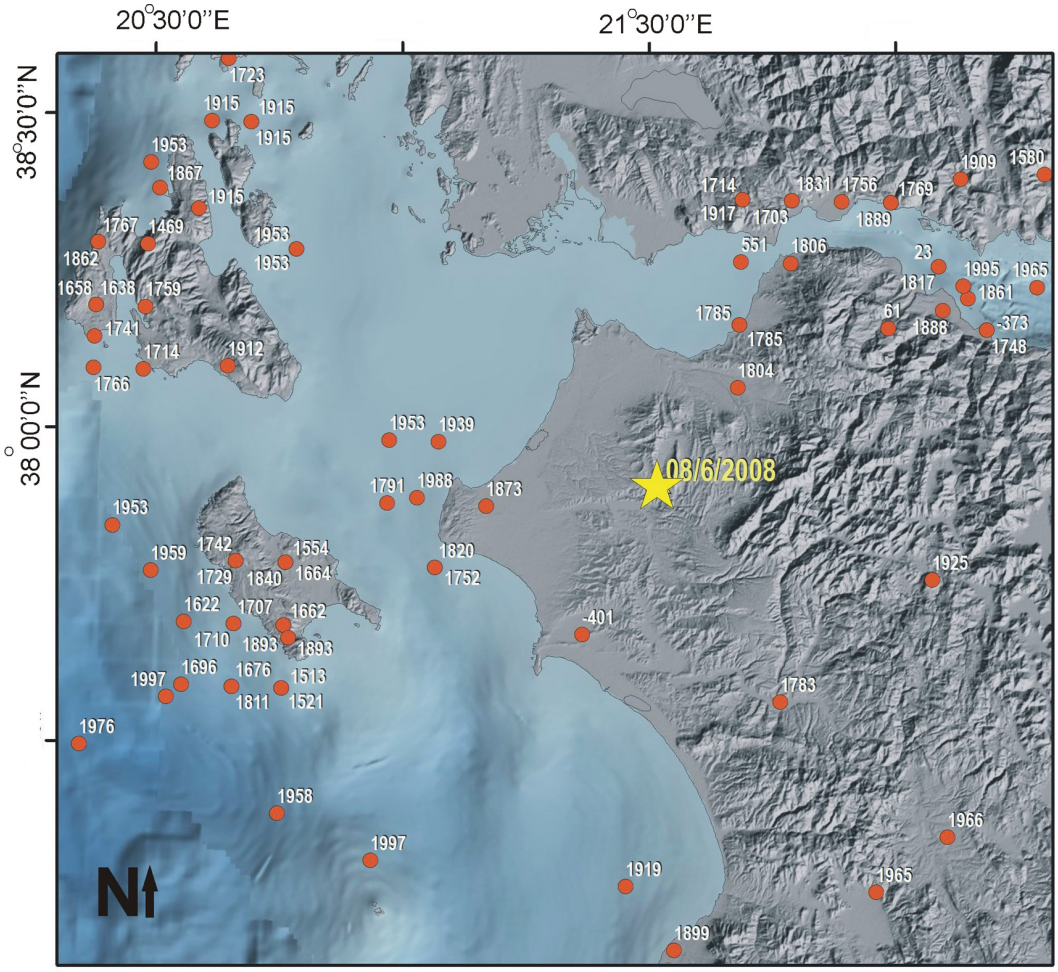

Figure 2. Map showing the distribution of earthquake's epicenters (for the period 1911-2007; M>5.5) in the broader area (red circles) and the location of June 8, 2008, earthquake epicenter (yellow star).

ized by two distinct tectonic stress regimes (i.e. bearing a vertical σ_1 and σ_3, respectively), the 2008 epicentral region is affected by a transcurrent regime where both maximum and minimum principal stress axes (σ_1 and σ_3) are subhorizontal and oriented nearly E-W and N-S, respectively [e.g. Hollenstein et al. 2008]. The causative fault with its subvertical setting, the NNE-SSW trend and the dextral strike-slip kinematics [e.g. Ganas et al. 2009, Koukouvelas et al. 2009] perfectly fits the seismotectonic behaviour of the area.

It should be noted however, that surface geology investigations suggest normal faulting as the most recent structures and no major active strike-slip faults have been documented so far. The apparent contradiction could be explained by a recent change of the regional stress field but more likely by the occurrence of a thick sequence of Triassic evaporites separating the two juxtaposed major tectonic units (Ionian and Gavrovo zones). This weak mechanical layer likely decoupled the uppermost rock volume from the deeper seismogenic one. It is indeed remarkable that the uppermost crust was lacking any seismic activity during the 2008 swarm, while all aftershocks were located below ca. 5 km and down to 20-25 km depth [Ganas et al. 2009, Papadopoulos et al. 2010, Kostantinou et al. 2011]. Also the slip distribution of the main shock as inferred from waveform analyses [Kostantinou et al. 2009] suggests that coseismic rupture stopped at ca. 5 km-depth.

3. Earthquake-induced environmental effects

Crustal earthquakes of moderate magnitude are common in western Greece and northwestern Peloponnesus [Benetatos et al. 2004]. In the recent past, other two similar events triggered liquefaction and rock-falls: the Vartholomio 1988 M = 5.5 and the Pyrgos 1993 m = 5.4 earthquakes (Figure 2). The former event triggered liquefaction phenomena such as ground fissures with ejection of sand-water mixture and sand volcanoes. According to Lekkas [1991] and Papadopoulos and Profis [1990], liquefaction-induced ground disruption was observed at the western bank of the river Pinios, about 400 m from the sea shore and east of Kastro village, while according to eyewitnesses, near Vartholomio water and sand were ejected from fissures creating sand craters with a diameter up to 60 cm.

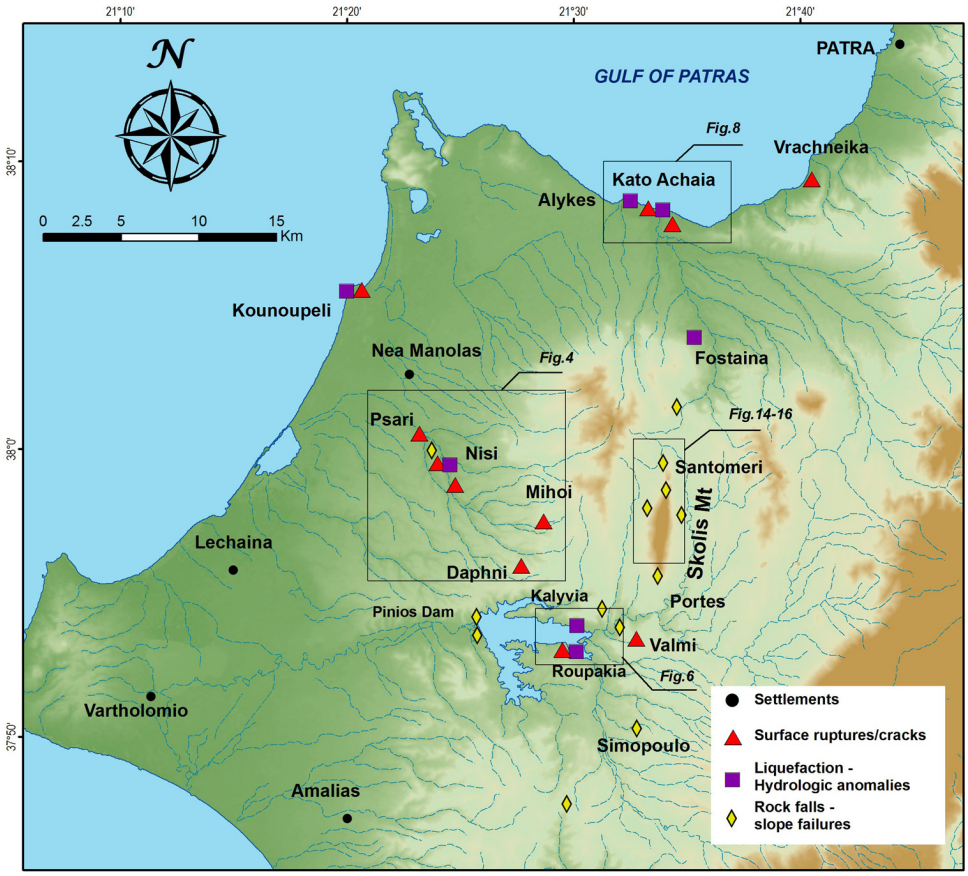

Figure 3. Ground failures triggered by the event of June 8, 2008, and mapped in the present investigation.

The latter event (Pyrgos, 1993) generated rock-falls and manifestations of soil liquefaction [Papadopoulos et al. 1994]. Rock-falls were observed in the area of the Fragapidima Monastery at an epicentral distance of 10 km not due to the main shock, but due to some major aftershocks [Papadopoulos et al. 1994]. Liquefaction related phenomena such as ejection of mixed sand and water from ground fissures with length up to 30 m and sand craters with diameters up to 50 cm were also observed in the area of Spiantza, close to the river Alfios [Lekkas 1994].

Also the June 8, 2008, earthquake was an 'areal morphogenic event' [Caputo 2005] because it generated characteristic co-seismic effects widespread in the broader epicentral region. The most severe ground failures were concentrated within three zones; i) close to the village Kato Achaia, where liquefaction manifestations and structural damages were reported, ii) at the foothills of Skolis Mountain, where large size rock falling phenomena occurred and iii) within a zone including the villages Nisi, Psari and Neapoli, where secondary surface ruptures and damages to buildings and infrastructures were observed (Figure 3).

The ground motion of the earthquake was also recorded by more than 21 strong motion instruments distributed around the ruptured fault segment [Margaris et al. 2008]. The highest values of the peak ground acceleration were recorded at the area of Pyrgos and Vartholomio towns corresponding to 0.19 g and 0.17 g, respectively (Table 1). Margaris et al. [2008] also suggest that the characteristics of the ground motion controlling the toppling of cemeteries features above-ground tombs (like crosses, photograph frames, and similar markings) were likely stronger at the northern end of the fault rupture than the southern one. In addition, the occurrence of large scale liquefaction phenomena and the deformation of the railway lines at Kato Achaia suggest that the peak ground acceleration in this area was significantly higher.

Site	Code	PGA (g)
Patras	PAT1	0.13
Patras	PAT2	0.11
Patras	PAT3	0.09
Vartholomio	VAR2	0.17
Pyrgos	PYR1	0.19
Zakynthos	ZAK2	0.04
Argostoli	ARG1	0.03

Table 1. Recorded values of the ground acceleration triggered by the earthquake of June 8, 2008 [Margaris et al. 2008].

Taking into account the descriptions of the ground deformations, we estimated the macroseismic intensity based on the definition of the ESI-2007 scale [Michetti et al. 2007]. The ESI-2007 scale was initially introduced as INQUA scale and the estimation of the degrees is achieved by taking into account the characteristics of the earthquake-induced environmental deformation including primary and secondary effects. The 2008 earthquake was classified as a reliable case study for the application of the ESI-2007 scale due to the fact that the environmental effects were widespread and well documented.

According to the ESI-2007 scale, the values of the macroseismic intensity range between V and VIII. In particular, the highest macroseismic intensity VIII was evaluated at the sites of Roupakia and Psari-Neapoli where large-scale liquefaction phenomena and diffuse secondary surface ruptures, respectively, were reported. The lowest intensity value was assigned at the site of Avgi on the shore of lake Pinios, where small-scale ground fissures were observed. Regarding the occurrence of soil liquefaction and slope instability phenomena, the evaluated intensity ranges from VI to VIII and from VI to VII, respectively. In areas, where muddy water was observed in boreholes, the intensity was evaluated as VI degree.

Table 2 lists the sites where the ESI-2007 scale was applied and the corresponding evaluated degree of macroseismic intensity.

Site	Type of failure	Latitude	Longitude	ESI-2007 scale
Alikes	Ejection of material	38° 09' 20. 99"	21° 32' 19 05"	VI
Alikes	Sand volcanoes	38° 09' 20. 03"	21° 32' 15. 34"	VI
Kato Achaia	Sand volcanoes	38° 09' 07. 86"	21° 33' 49. 15"	VII
Kato Achaia	Sand volcanoes	38° 08' 48. 87"	21° 33' 36. 77"	VII
Kato Achaia	Railroad deformation	38° 08' 45. 66"	21° 33' 40. 81"	
Kato Alissos	Cracks on bridge	38° 08' 40. 42"	21° 34' 08. 61"	
Vrahneika	Cracks on the pavement	38° 10' 21. 72"	21° 40' 31. 68"	
Araxos	Muddy water in boreholes	38° 09' 33. 90"	21° 25' 19. 61"	VI
Neapoli	Muddy water in boreholes	38° 01' 07. 97"	21° 24' 53. 89"	VI
Karamesineika	Broken water pipeline	38° 06' 05. 16"	21° 30' 32. 46"	
Psari – Neapoli	Surface rupture	38° 01' 01. 65"	21° 24' 04. 19"	VIII
Nisi	Liquefaction	38° 00' 58. 82"	21° 24' 18. 58"	VI
Nisi	Small scale landslide	38° 00' 31. 71"	21° 24' 25. 75"	VI
Neapoli	Normal fault	38° 00' 29. 40"	21° 24' 25. 84"	VII
Mihoi	Surface ruptures	37° 57' 53. 75"	21° 29' 12. 75"	VII
Mihoi	Surface ruptures	37° 58' 02. 89"	21° 29' 18. 09"	VII
Santomeri	Rock falls	37° 59' 19. 85"	21° 34' 29. 25"	VII
Santomeri	Rock falls	37° 59' 46. 49"	21° 34' 30. 59"	VII
Kalivia	Small scale liquefaction	37° 54' 21. 73"	21° 31' 14. 95"	VI
Valmi	Landslide	37° 54' 13. 85"	21° 32' 41. 45"	VII
Roupakia	Sand volcanoes	37° 53' 51. 83"	21° 30' 50. 47"	VIII
Avgi	Small ground fissures	37° 51' 45. 78"	21° 28' 26. 14"	V
Pinios river	Ejection of material	37° 50' 39. 84"	21° 32' 17. 74"	VI
Glyfa	Damaged boreholes	37° 50' 38. 65"	21° 08' 33. 40"	
Vartholomio	Damaged boreholes	37° 51' 49. 04"	21° 12' 20. 92"	

Table 2. Degrees of the seismic intensity that were evaluated based on ESI-2007 scale. The description of the environmental effects can be found in Section 3.

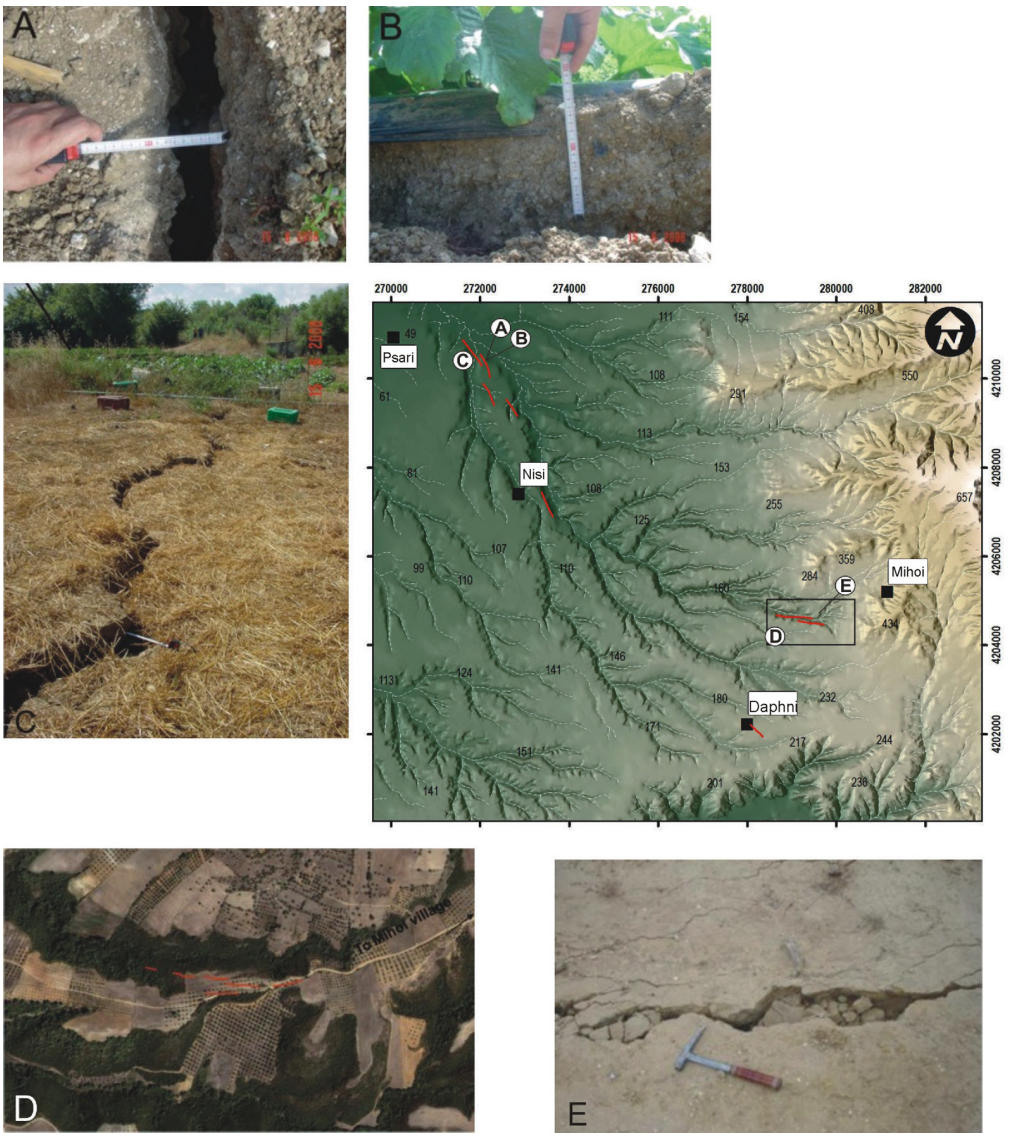

Figure 4. Surface ruptures close to the villages of Psari and Mihoi.

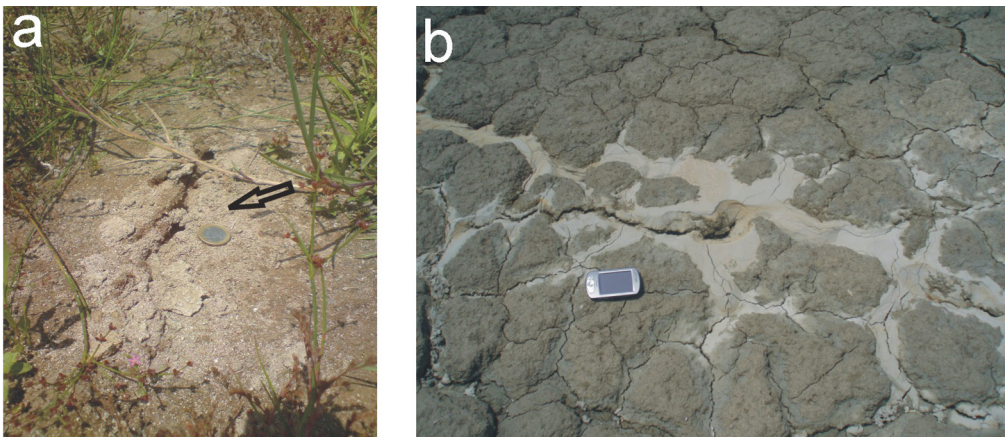

Figure 5. (a) Ejection of sand-water mixture at the banks of Pinios River; (b) ejection of sand-water mixture at the shore of Pinios Lake (site Kalivia).

3.1. Coseismic ground failures

The mapped secondary surface ruptures are mainly concentrated along two alignments; the Psari-Nisi line and Michoi line. The former is more than 5 km-long, is oriented NNW-SSE and consists of open ground fractures with local normal and strike-slip kinematics. They form a left-stepping en-echelon geometry and generally follow the adjacent river scarp (Figure 4).

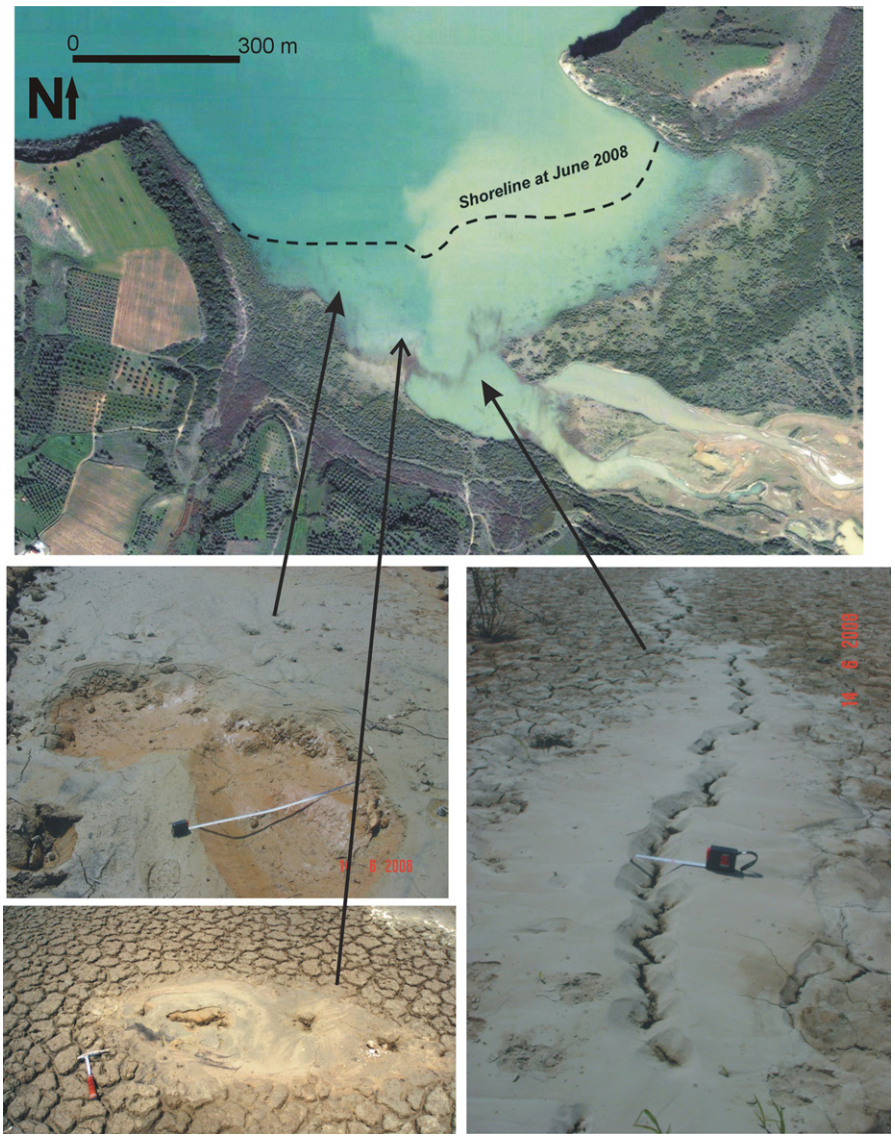

Figure 6. Liquefaction manifestation at the area of Roupakia. Sand craters with a diameter up to 85 cm (top left); Vent fractures 85 cm (right); Sand volcanoes (bottom left).

A shear zone with no significant vertical displacement coincides with the general strike of the surface ruptures. It is also associated with liquefaction and slope movements along its strike.

The Michoi lineament was mapped close to the epicentre, where a rather long (>2 km) ground fractures system trending WNW-SSE was observed in the hills west of Michoi village (Figure 4). It forms a deformation zone of up to 6 m-wide and it is also associated with rock-falls and landslides.

3.2. Liquefaction features

Liquefaction-induced ground manifestations have been reported in many places as it is shown in Figure 3 and listed in Table 2. Clear evidences of liquefaction such as sand volcanoes and vent fractures were observed both at the areas located to the north (Kato Achaia, Alikes, and Nisi) and to the south (at the banks of the river Pinios and at the shore of Pinios Lake). These liquefaction-induced ground failures appeared to be concentrated in areas characterised by alluvial deposits (Figure 1). In particular, at the banks of the Pinios River, small-scale ground cracks were observed and granular material was ejected while 1-2 cm-wide opening features were generated towards the river (Figure 5a). Close to this site, in Kalivia village, fine-grained material was ejected from ground fissures as shown in Figure 5b.

Liquefaction phenomena were also reported along the shore of the Pinios Lake, close to the village Roupakia, about 9 km from the NOA epicentre (Figures 1 and 6). At this site, typical examples of liquefaction surface evidences were observed such as i) sand-mud craters with diameter up to 85 cm and smaller ones with diameter up to 70 cm (Figure 6b), ii) vent fractures with length more than 5 m and width up to 15 cm (Figure 6c) and iii) sand volcanoes with diameter up to 17 cm (Figure 6d). Some lateral spreading at the banks of the river was additionally observed.

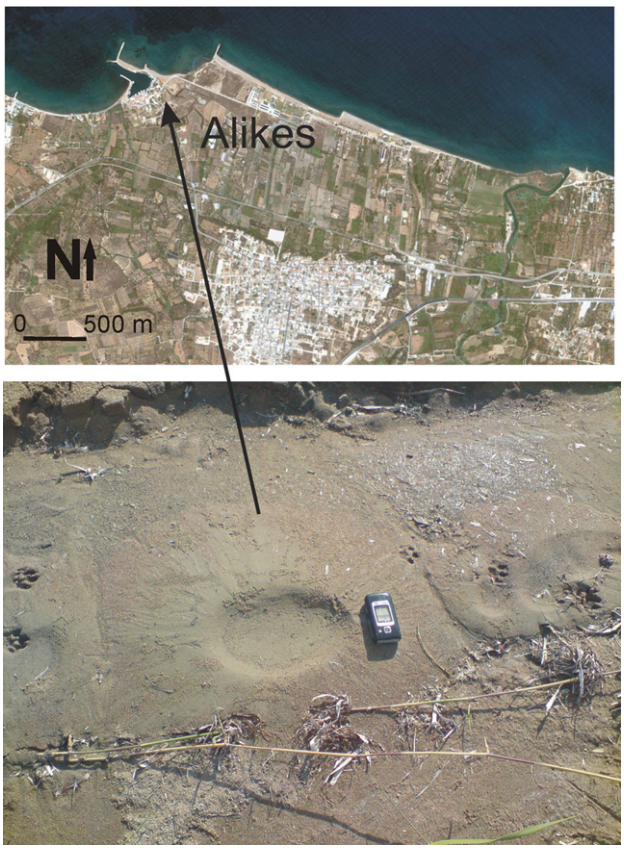

Figure 7 (left, top to bottom). Liquefaction manifestations at the sea shore of the village Kato Achaia. (a) General view of the area; (b,c,d) examples of vent fractures with 12, 20 and 30 cm-width, respectively; (e) formation of a 4 m-long vent fracture.

Figure 8 (above, top to bottom).Map showing the location of liquefaction-induced ground disruption sites in the area of Alikes. Example of sand crater with a diameter of 15 cm formed at the site Alikes.

Liquefaction phenomena occurred also at several sites located north of the epicentre. The most impressive ones were mapped along the sea shore near the village Kato Achaia, at an epicentral distance of ca. 20 km (Figure 7), where ejected sandy grey material formed vent fractures from 50 cm- to 4 m-long and up to 22 cm-wide as well as sand volcanoes up to 8 cm in diameter. Furthermore, ejection of grey sand was observed at a distance of 600 m from the coast line (offshore).

Sand volcanoes and small scale lateral spreading phenomena were also examined close to the river mouth of a torrent near Alikes (Figure 8), ca. 2 km west of Kato Achaia village. The diameter of the sand volcanoes ranged from 4 to 12 cm, while from small scale cracks on the pavement, sandy material was locally ejected.

In addition, close to the Nisi village, a surface rupture showing 20 cm of throw and 18 cm of heave was mapped and a small sand volcano has been reported by Koukouvelas et al. [2009].

Finally, structural damages that were possibly caused by differential soil subsidence, are documented at the waterfront area of the village Vrachneika, at an epicentral distance of 25 km. In this area, the pavement was cracked and buried water pipes were damaged. The mean direction of the cracks was parallel to the coastline while their measured length was up to 500 m. The horizontal displacement ranged from 3 to 7 cm while in some places a throw of 3 cm was also reported (Figure 9). It should be noted that no evidence of liquefaction phenomena such as ejection of material from the cracks and/or creation of sand volcanoes was observed at this area.

The susceptibility to liquefaction at these sites has been further investigated by correlating the epicentral distance with the earthquake magnitude. The maximum epicentral distances of the liquefied sites, estimated according to the epicentre's coordinates by both National Observatory of Athens (NOA) and Aristotle Univeristy of Thessaloniki (AUTh) (Figure 1), were correlated to the magnitude of the event using the regressions proposed by Papathanassiou et al. [2005] and Ambraseys [1988]. It is noteworthy that all sites where liquefaction phenomena have been documented by the present research fall within the maximum epicentral

Figure 9. Structural damages at the waterfront area of the village Vrahneika. Examples of failures on pavement with both throw and opening components (left: throw = 3 cm and opening = 2 cm; right: opening = 4 cm).

distance for a 6.4 magnitude event (Figure 10).

During the field work, samples of ejected material were collected from sand craters and vent fractures in the areas of Kato Achaia and Roupakia and were analyzed in the Laboratory of Engineering Geology and Hydrogeology of the Department of Geology at the Aristotle University of Thessaloniki, in order to define their grain size distribution. The three collected samples from the shore of the Pinios Lake, are classified as silty sand (SM) since the fine-grain content of these deposits are 24%, 30% and 21%, respectively. The material that was collected from vent fractures and sand boils in Kato Achaia is classified as poorly graded sand; the content of clay and silt being 8% and 5%, respectively. Based on these results, the sediments in these areas can be characterized as susceptible to liquefaction.

3.3. Earthquake-induced slope failures

The 2008 earthquake also triggered several landslides and rock-fall phenomena in localities prone to sliding south-east of the epicentre. Following earlier studies, earthquake-induced slope instabilities are concentrated in specific zones depending on the bedrock geology, the morphology and topography of the area as well as anthropogenic factors [Owen et al. 2008]. Furthermore, smaller scale phenomena were reported in a wider area into the epicentral zone.

The most severe slope failure phenomena were rock-falls, confirming the conclusion of Keefer [1984] that under seismic conditions the most susceptible to slope failure initiation are rock-falls and rock-slides. The characteristics of the rock-falls, described by Keefer [1984], are movements of bounding, rolling or free falling high velocity blocks and boulders with commonly a shallow depth (less than 3 m) sliding surface. In the following, a brief description of the observed slope failures observed within the epicentral area is presented including a map (Figure 3) of their spatial distribution.

A preliminary evaluation of the rock-fall hazard within an area can be achieved by correlating the expected earthquake magnitude with the epicentral distance of the landslide prone zone. Several works have been published correlating these two parameters, among them Keefer [1984] suggests that rock-falls can be triggered by magnitudes M>4.0 and that disrupted slides and falls can be generated by ground shaking weaker than for lateral spreads or flows. According to the classification proposed by Keefer [1984], rock-falls, rock-slides, soil-falls and disrupted soil-slides have the lowest triggering threshold ground motion. Regarding the area of Greece, Papadopoulos and Plessa [2000] compiled a dataset of 47 earthquake-induced landslides where the magnitude (M_s) of causative events ranges between 5.3 to 7.9 with peaks at M_s=6.4 and 6.7. Based on these suggestions, the study area should be classified as highly susceptible since the magnitude of the June 8, 2008, was M_w=6.4 (roughly equivalent to M_s=6.4; Papazachos et al. [1997]) and the slope instabilities were expected to be rock-falls and rock-slides

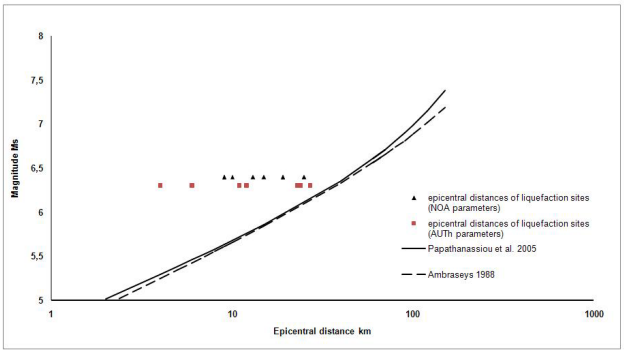

Figure 10. Distribution of the liquefied sites based on their epicentral distance and comparison to the upper bound curves proposed by Papathanassiou et al. [2005] and Ambraseys [1988] for the assessment of liquefaction susceptibility.

Figure 11. Example of large size rock-fall in the village of Santomeri.

Figure 12. Slope failure close to the village of Valmi.

due to the geological and geomorphological characteristics of the area.

At both western and eastern slopes of Skolis Mountain, rock-toppling phenomena of large dimensions, accompanied by small rock-slides, were observed in steep slopes developed in limestone. The volume of the rock-falls was up to 8 m^3, causing damages to houses at the village Santomeri (Figure 11) and to the road network. In particular, large size craters up to 2 m in diameter were observed on pavemented roads as well as north of Santomeri village. Consequently, the local authorities demanded the evacuation of three villages, including Santomeri, for three days following the main shock in order to avoid possible casualties from the possible re-activation of rock-falls during the aftershocks sequence.

At the area of the Pinios Lake, cracks on top of a slope were also reported parallel to the shoreline causing a small movement towards the lake.

Furthermore, landslides were reported close to the village Nisi (see Figure 3 for location). In both cases, the ground failure was induced by the sandy non-cohesive material of the slope. Along the road Valmi-Portes, close to the village of Valmi, a large-scale landslide was reported along a slope consisting of marls and sandstones (Figure 12). According to Margaris et al. [2008], the failure is associated with pre-existing sub-vertical fractures and/or planes of weakness affecting the rock mass and trending sub-parallel to the slope strike.

Smaller scale landslides were finally reported in many other places but without causing any severe damage. In particular, the National Road Patras-Pirgos was closed for few hours after the main shock in order to remove small dimensions blocks, while similar phenomena were observed at Kato Achaia village. According to Margaris et al. [2008], further landslides were triggered along the National Road Diakofto-Kalavrita (Pounta), 50 km N-NE trending of the macroseismic epicentre.

3.4. Assessing the run-out distances of rock-falls at Skolis Mountain

Among the aims of this study is the evaluation of the rock-fall hazard at the foothills of Skolis Mountain and to estimate the run-out distance of rock-fall events. The prevailing lithologies within the study area are limestone and flysch (Figure 13).

Based on topographic data, a Digital Elevation Model was created (Figure 13), with 20 m-resolution. From the DEM a map with the distribution of the slope angle was also compiled. The elevation of the slope is up to 974 m and the slope angle varies between 30° and 64° (Figure 14).

For the same area, a geological map was compiled at the 1:50,000 scale based on original field work and literature data [Fleury et al. 1981]. In Figure 14, the locations of the fallen blocks generated by the June 2008 event are shown.

In order to estimate the run-out distance of boulders, empirical rock-fall models were developed based on the relationship between topographic factors and the length of the run-out zone [Dorren 2003]. The parameters commonly used to describe the rock-fall run-out zone are the angle or the horizontal distance [Petje et al. 2005]. The evaluation of the run-out of a rock-fall represents a crucial parameter, particularly for urban planners, for better estimating the hazard within a specific area.

In general, two methods are mainly applied for the estimation of the maximum distance that a boulder can reach. The first model, commonly referred to as *Fahrboschung angle*, was suggested by Heim [1932] and Onofri and Canadian [1979]. It predicts the run-out zone using the angle between the horizontal and the line ideally connecting the top scar of a rock-fall source with the stopping point for any given rock-fall event. According to the Onofri and Canadian [1979] approach, the limits of the Fahrboschung angle determined for

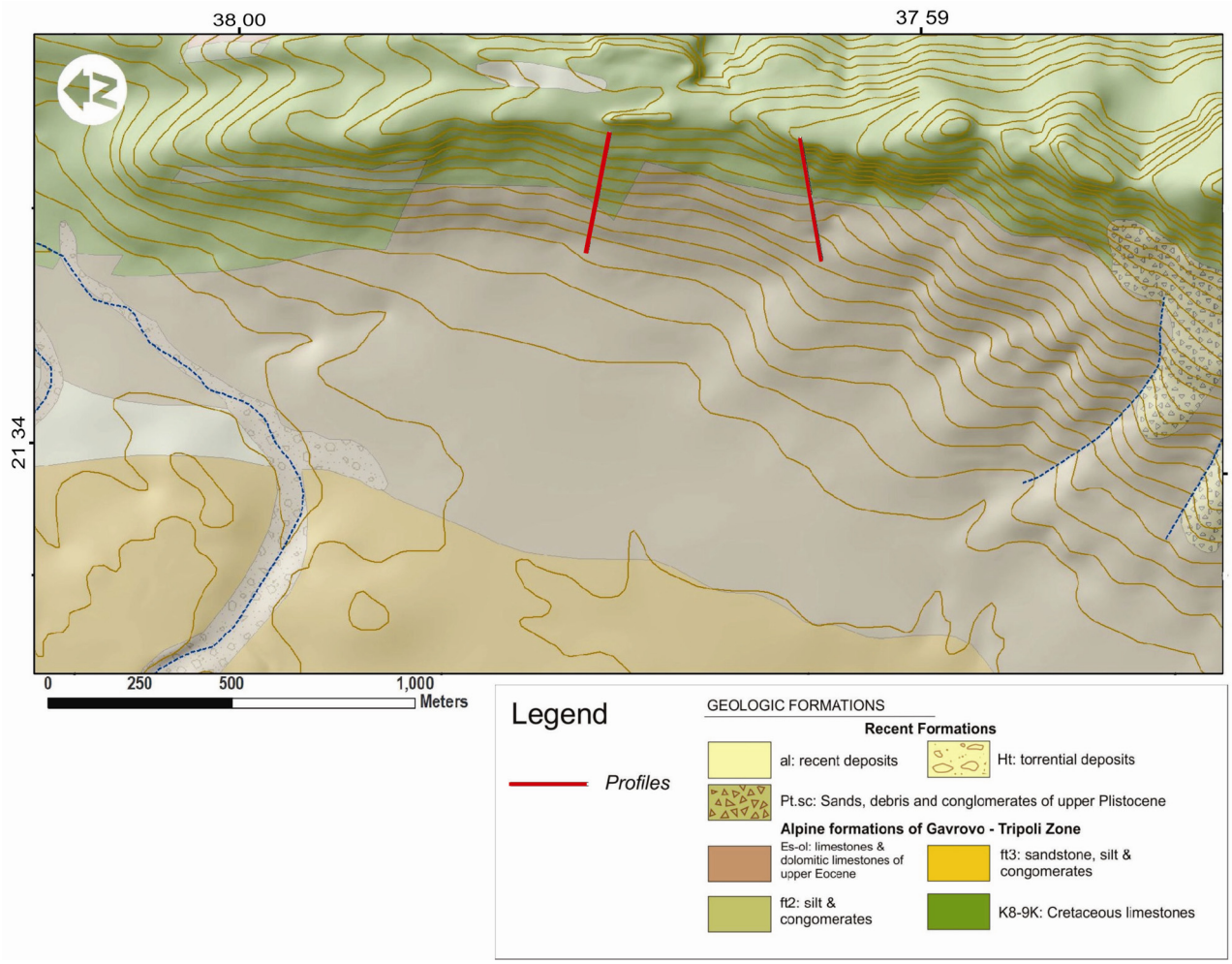

Figure 13. Geological map of the area of Skolis Mountain (contour lines: 20 m).

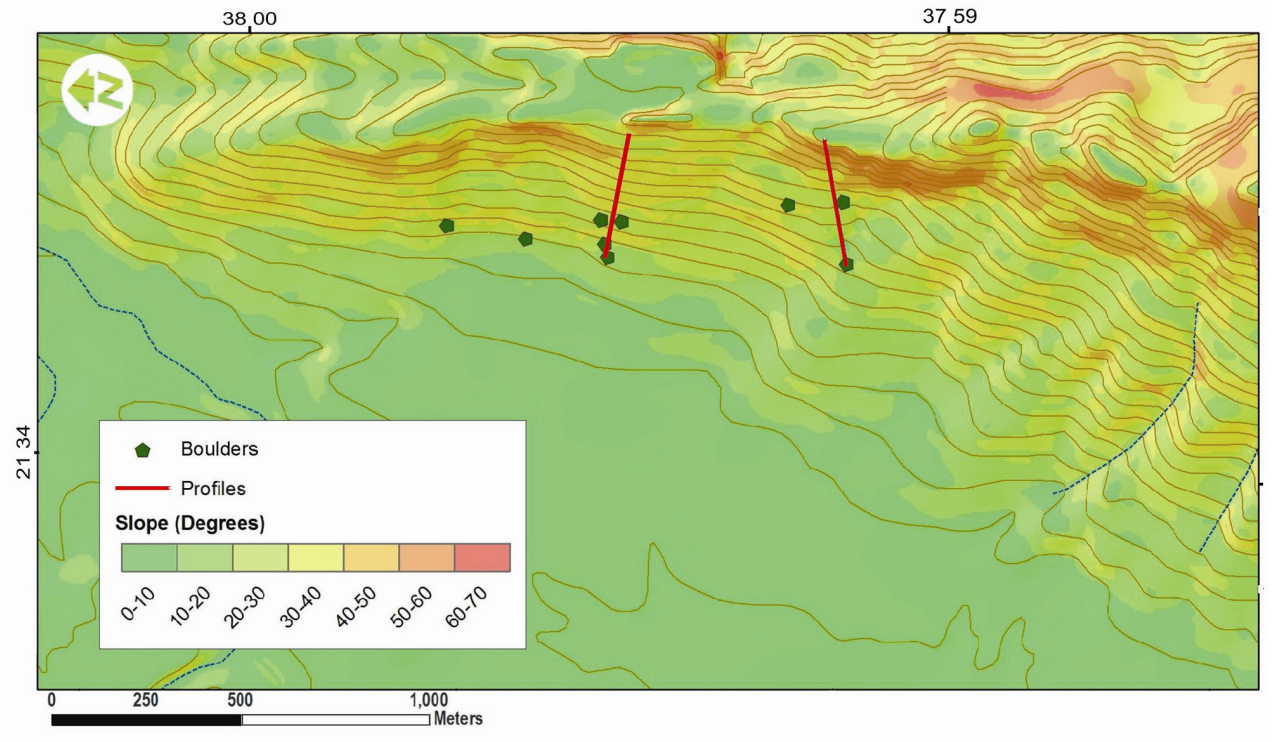

Figure 14. Slope map of the study area showing the location of boulders and the profiles used for evaluating the rock-fall hazard in this study (contour lines: 20 m).

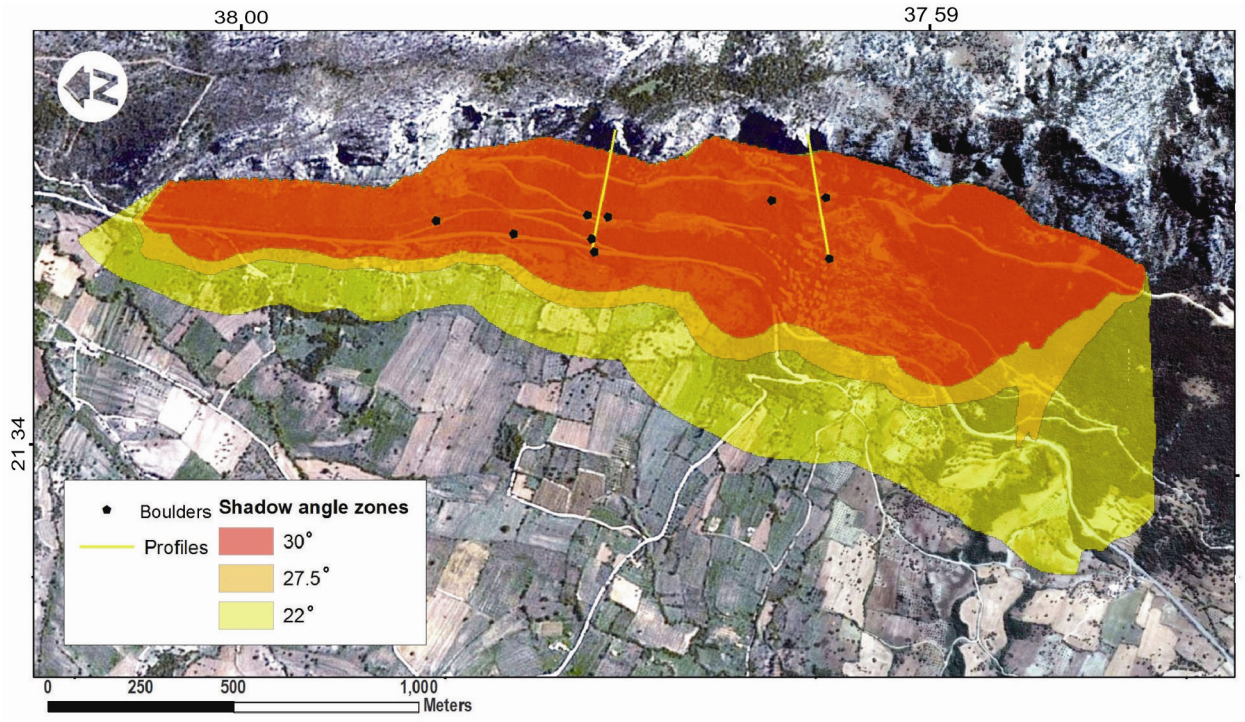

Figure 15. Shadow angle zones delineated using the values of 30°, 27.5° and 22°, respectively.

the Skolis Mountain slope are 28.3° and 40.7°, while the 50% of the boulders stopped within 33.5° and 72% stopped within 32°.

The second methodological approach is known as *minimum shadow angle* and was proposed by Evans and Hungr [1993] mainly based on Lied's [1977] work. According to these authors, the area downslope the base of a talus reached by large size boulders is termed the 'rock-fall shadow zone'. Accordingly, the equivalent shadow angle is defined as the angle between the outer margin of the shadow zone and the apex of the detritic cone. The distal part of the shadow zone often contains only very few boulders, which are sparsely distributed on the surface [Evans and Hungr 1993]. The major difference with the previous empirical model is that this approach does not require the measurement of the starting and the end points of each fallen block. Evans and Hungr [1993], having investigated 16 talus slopes in British Columbia, suggested that a minimum shadow angle of 27.5° is adequate for a preliminary estimation of a rock-fall run-out distance, while Dorren [2003] having compared the outcomes of several studies, propose an angular range between 22° and 30°. According to Petje et al. [2005] where the slope of the talus is smooth, even lower angular values should be taken into account (23°-24°).

For the purpose of our investigation, the shadow angle method is preferred, because it is more reliable at a larger scale [Meibl 2001, Copons et al. 2004] and it is also more suitable comparing to the Fahrboschung angle model which predicts an extremely long travel distance [Evans and Hungr 1993, Wieczorek et al. 1999]. Taking into consideration the proposed angular values, maps of run-out distances were compiled and compared to the locations of the fallen rocks. Following a detailed geological survey carried out few days after the earthquake, it was possible to measure the distance between numerous fallen boulders and the lower limit of the outcropping limestone. As it is shown in Figure 15, the run-out distances of the boulders are within the zone delineated by a shadow angle of 30°, showing a good performance of the model.

4. Concluding remarks

The earthquake of June 8, 2008, caused severe ground effects that were widespread in the northwestern part of Peloponnesus, Greece. Liquefaction manifestations and rock-fall phenomena were generated by the event and caused damages to lifelines and houses particularly along, or close to, the surface projection of the causative fault.

A catalogue of earthquake-induced ground deformation and a map showing their spatial distribution is presented in this work, while an assessment of the potential of geological hazard (soil liquefaction and slope instability) within two areas, Kato Achaia and Santomeri villages has been also performed. A major outcome of this investigation indicates that the distribution of the earthquake-induced rock-falls at the foothills of Skolis Mountain are in agreement with, and could be thus predicted by, the run-out distance models. Accordingly, these empirical models could be used in advance, firstly,

for delineating areas prone to slope instability, secondly, for applying safety devices and precautionary measures and eventually to prevent possible structural damages or human losses. In addition, the prone to liquefaction zones and their potential degree could also be recognized and defined using available methodological approaches regarding the preliminary evaluation of the susceptibility to liquefaction of the geological units based on their epicentral distances and the grading characteristics of the soil layers. All this will contribute in mitigating the seismic risk.

References

Ambraseys, N.N. (1988). Engineering seismology, Int. J. Earthq. Eng. Struct. Dyn., 17, 1-105.

Benetatos, C., A. Kiratzi, C. Papazachos and G. Karakaisis (2004). Focal mechanisms of shallow and intermediate depth earthquakes along the Hellenic Arc, J. Geodyn., 37, 253-296.

Caputo, R. (2005). Ground effects of large morphogenic earthquakes, J. Geodyn., 40 (2-3), 113-118.

Chouliaras, G. (2009). Seismicity anomalies prior to 8 June 2008, M_w=6.4 earthquake in Western Greece, Nat. Hazards Earth Sys., 9 (2), 327-335.

Copons, R., J.M. Vilaplana, J. Corominas, J. Altimir and J. Amigo (2004). Rockfall risk management in high density urban areas. The Andorran experience, In: T. Glade, M. Anderson and M. Crozier (eds.), Landslide Hazard and Risk, John Wiley & Sons, 675-699.

Dorren, L.A. (2003). Review of rockfall mechanics and modelling approaches, Prog. Phys. Geog., 27, 69-87.

Evans, S.G., and O. Hungr (1993). The assessment of rock fall hazard at the base talus slopes, Can. Geotech. J., 30, 620-636.

Feng, L., A.V. Newman, G.T. Farmer, P. Psimoulis and S. Stiros (2010). Energetic rupture, coseismic and post-seismic response of the 2008 M_w 6.4 Achaia-Elia Earthquake in northwestern Peloponnese, Greece: an indicator of an immature transform fault zone, Geophys. J. Int., 183, 103-110.

Fleury, J.J., P. De Wever, A. Izart and J. Dercourt (1981). Goumero Sheet, Gelogical Map of Greece in scale of 1:50.000, Institute of Geology and Mineral Exploration, Athens.

Gallovic, F., J. Zahradnik, D. Krızova, V. Plicka, E. Sokos, A. Serpetsidaki and G-A. Tselentis (2009). From Earthquake Centroid to Spatial-Temporal Rupture Evolution: M_w 6.3 Movri Mountain Earthquake, June 8, 2008, Greece, Geophys. Res. Letters, 36 (21), 1-5.

Ganas, A., E. Serprlloni, G. Drakatos, M. Kolligri, I. Adamis, Ch. Tsimi and E. Batsi (2009). The M_w 6.4 SW-Achaia (Western Greece) Earthquake of 8 June 2008: Seismological, Field, GPS observations, and Stress Modelling, J. Earthq. Eng., 13 (8), 1101-1124.

Hageman, J. (1976). Stratigraphy and sedimentary history of the Upper Cenozoic of the Pyrgos area (Western-Peloponnesus), Greece, Annales Géologiques des Pays Helléniques, 28, 299-333.

Heim, A. (1932). Bergsturz und menschenleben, Beiblatt zur Vierteljahrsschrift der Naturforschenden Gesellschaft in Zurich, 77, 1-218.

Hollenstein, Ch., M.D. Muller, A. Geiger and H.-G. Kahle (2008). Crustal motion and dformation in Greece from a decade of GPS measurements, 1993-2003, Tectonophysics, 449, 17-40.

Kamberis, E., S. Sotiropoulos, O. Aximniotou, S. Tsaila-Molopoli and C. Ioakim (2000). Late Cenozoic deformation of the Gavrovo and Ionian zones in northwestern Peloponnesos (Western Greece), Annali di Geofisica, 43 (5), 905-919.

Keefer, D. (1984). Landslides caused by earthquakes, Geol. Soc. Am. Bull., 95, 406-421.

Kokkalas, S., E. Kamberis, P. Xypolias, S. Sotiropoulos and I. Koukouvelas (2013). Coexistence of thin- and thick-skinned tectonics in Zakynthos area (western Greece): Insights from seismic sections and regional seismicity, Tectonophysics, 597-598, 73-84.

Konstantinou, KI., N.S. Melis, S.-J. Lee, C.P. Evangelidis and K .Boukouras (2009). Rupture process and aftershocks relocation of the 8 June 2008 M_w 6.4 earthquake in northwest Peloponnese, western Greece, B. Seismol. Soc. Am., 99 (6), 3374-3389.

Konstantinou, K.I., C.P Evangelidis and N.S Melis (2011). The 8 June 2008 M_w 6.4 earthquake in northwest Peloponnese, western Greece: A case of fault reactivation in an overpressured lower crust?, B. Seismol. Soc. Am., 101 (1), 438-445.

Koukouvelas, I., S. Kokkalas and P. Xypolias (2009). Surface deformation during the M_w 6.4 (8 June 2008) Movri Mountain earthquake in the Peloponnese, and its implications for the seismotectonics of western Greece, Int. Geol. Rev., 52 (2), 249-268.

Lekkas, E. (1991). Macroseismic observations alter the earthquake of October 16th 1988 in Killini peninsula (NW Peloponnesus), Bulletin of the Geological Society of Greece, 20, 313-328.

Lekkas, E. (1994). Liquefaction risk zonation and urban development at western Peloponnesus, In: 7th International IAEG Congress, Lisboa, Proceedings, 2095-2102.

Lied, K. (1977). Rock fall problems in Norway, In: Rockfall dynamics and protective work effectiveness, ISMES publ. No. 90, Bergamo, 51-53.

Margaris, B., C. Papaioannou, N. Theodoulidis, A. Savvaidis, N. Klimis. K. Makra, C. Karakostas, V. Lekidis,

T. Makarios, T. Salonikios, M. Demosthenus, G. Athanasopoulos, G. Mylonakis, C. Papantonopoulos, V. Efthymiadou, P. Kloukinas, I. Ordonez, V. Vlachakis and J.P. Stewart (2008). Preliminary report on the principal seismological and engineering aspects of the M_w=6.5 Achaia-Ilia (Greece) earthquake on 8 June 2008, GEER Association Report No. GEER-013 2008.

Mavromatidis, A. (2009). Review of hydrocarbon prospectivity in the Ionian Basin, Western Greece, Energy Sources Part A, 31, 619-632.

Meibl, G. (2001). Modeling the runout distances of rock falls using a geographic information system, Zeitschrift für Geomorphologie. Supplementband, 125, 129-137.

Michetti, A.M., E. Esposito, L. Guerrieri, S. Porfido, L. Serva, R. Tatevossian, E. Vittori, F. Audemard, T. Azuma, J. Clague, V. Comerci, A. Gurpinar, J. MC Calpin, B. Mohammadioun, N.A. Morner, Y. Ota, E. Roghozin (2007), Intensity Scale ESI 2007, In: L. Guerrieri and E. Vittori (eds.), Memorie descrittive della Carta Geologica d'Italia, vol. 74, Servizio Geologico d'Italia - Dipartimento Difesa del Suolo, APAT, Rome, Italy.

Onofri, R., and C. Candian (1979). Indagine sui limiti di massima invasione dei blocchi franati dovuti al sisma del Friuli del 1976. Considerazione delle opere di difesa, Pubbl. Regione Autonome Friuli-Venezia Giulia e Università di Trieste, Istituto di Geologia e Paleontologia, Trieste, 42 pp.

Owen, L., U. Kamp, G. Khattak, E. Harp, D. Keefer and M. Bauer (2008). Landslides triggered by the 8 October 2005 Kashmir earthquake, Geomorphology, 94, 1-9.

Papadopoulos, A.G., and Th. Profis (1990). Macroseismic observations related with the strong shock of October 16th, 1988, in NW Peloponnesus Greece: the important role of the microzonation conditions, J. Geodyn., 12, 217-231.

Papadopoulos, G.A., D. Fountoulis and K. Grivas (1994). The 26 March 1993 earthquake in the area of Pyrgos, NW Peloponnesus, Greece: Earthquake engineering aspects, In: G. Papadopoulos and K. Makropoulos (eds), 2nd workshop statistical models and methods in seismology applications on prevention and forcasting of earthquakes, Cephalonia, Greece, 208-235.

Papadopoulos, G.A., and A. Plessa (2000). Magnitude - distance earthquake - induced landslides in Greece, Eng. Geol., 58, 377-386.

Papadopoulos, G.A., V. Karastathis, C. Kontoes, M. Charalampakis, A. Fokaefs and I. Papoutsis (2010). Crustal deformation associated with east Mediterranean strike-slip earthquakes: The 8 June 2008 Movri (NW Peloponnese), Greece, earthquake (M_w 6.4) Tectonophysics, 492 (1-4), 201-212.

Papathanassiou, G., S. Pavlides, B. Christaras and K. Pitilakis (2005). Liquefaction case histories and empirical relations of earthquake magnitude versus distance from the broader Aegean Region, J. Geodyn., 40, 257-278.

Papazachos, B.C., A.A. Kiratzi and B.G. Karakostas (1997). Toward a homogeneous moment magnitude determinatio in Greece and surrounding area, B. Seismol. Soc. Am., 87, 474-483.

Petje, U., M. Ribičič and M. Mikoš (2005). Computer simulation of stone falls and rockfalls, Acta geographica Slovenica, 45 (2), 93-120.

Tsoflias, P. (1970). Geological structure of the northern part of Peloponnese (Achaia County), Annales Géologiques des Pays Helléniques, 21 1-554.

Wieczorek, G.F., M.M. Morrisey, G. Iovine and J. Godt (1999). Rock-fall potential in the Yosemite Valley, California, USGS Open file report, 99-578.

*Corresponding author: George Papathanassiou,
Aristotle University of Thessaloniki, Department of Geology, Thessaloniki, Greece; email: gpapatha@auth.gr.